

Measurement of the Muonic X-Ray Cascade in Metallic Iron

F. J. Hartmann, T. von Egidy, R. Bergmann, M. Kleber, H.-J. Pfeiffer, K. Springer, and H. Daniel
Physics Department, Technical University of Munich, Munich, Germany
 (Received 26 January 1976)

The muonic x-ray cascade in Fe has been measured with Ge detectors. The intensities of 103 x-ray lines from the *K*, *L*, *M*, *N*, and *O* series were determined and compared with cascade calculations. The best "initial distribution" at principal quantum number $n = 20$ does not strongly depend on the angular momentum.

In most experiments on muonic x rays performed so far^{1,2} lines originating from upper states of principal quantum number $n_u \lesssim 10$ have been observed. The highest value reported³ is $n_u = 16$. Usually a certain "initial distribution" at a fixed principal quantum number n_i is assumed and the calculated Auger and x-ray cascade is compared with the experiment; most investigators start with $n_i = 14$ and assume either a "statistical distribution"

$$P_l \propto 2l + 1, \quad (1)$$

where l is the orbital angular momentum quantum number, or a "modified statistical distribution"

$$P_l \propto (2l + 1)e^{\alpha l}, \quad (2)$$

where α is treated as a free parameter.

In the present paper we report on a measurement of the muonic x-ray spectrum for metallic iron in the energy range from 3 to 1900 keV. The cascade was determined as completely as possible in order to allow the first comprehensive test

of theoretical models.^{1,3-6} The experiment was performed at the superconducting muon channel at Schweizerisches Institut für Nuklearforschung at Villigen, Switzerland. The target consisted of a $50 \times 70 \times 1.0$ mm³ pure-iron metal sheet and was tilted to the beam yielding a thickness of 2.0 mm in the direction of the beam axis. X-ray spectra were taken simultaneously with a 0.5-cm³ intrinsic Ge detector (in-beam resolution 0.38 keV full width at half-maximum at 14.0 keV) and with a 42-cm³ Ge(Li) detector (2.4 keV at 1.25 MeV), analyzed with 8192-channel analog-to-digital converters, and recorded with an on-line computer; a 4096-channel analyzer was used to record the ungated spectra, in order to survey the coincidence electronics. The distribution of the muon stops in the target was measured with the help of the induced radioactivity (⁵⁶Mn). Part of a spectrum is shown in Fig. 1.

Screening corrections were calculated with the Bohr-Sommerfeld method⁷ using a potential obtained from published numerical values⁸ extra-

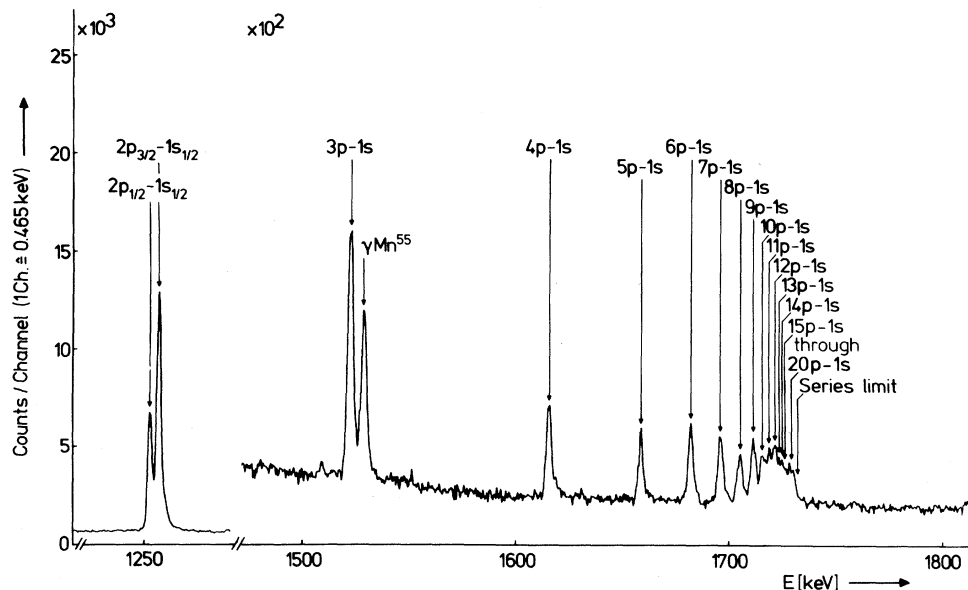


FIG. 1. Muonic x-ray spectrum of the *K* series in Fe.

TABLE I. Experimental and calculated intensities of the muonic K and L series in iron (per 100 stopped muons).

n	K-Series		L-Series										
	np \rightarrow 1s $_{1/2}$ exp.	np \rightarrow 1s $_{1/2}$ calc.	ns \rightarrow 2p $_{1/2}$ exp.	ns \rightarrow 2p $_{3/2}$ exp.	ns \rightarrow 2p exp.	ns \rightarrow 2p calc.	np \rightarrow 2s exp.	np \rightarrow 2s calc.	nd \rightarrow 2p $_{1/2}$ exp.	nd \rightarrow 2p $_{3/2}$ exp.	nd \rightarrow 2p exp.	nd \rightarrow 2p calc.	
2p $_{1/2}$	24.53 \pm 0.78	74.07											
2p $_{3/2}$	47.08 \pm 1.45												
3	8.17 \pm 0.25	7.17	0.42 \pm 0.05	0.80 \pm 0.30 ^a	1.22 \pm 0.30	1.22	1.21 \pm 0.10	1.36	15.49 \pm 0.63	28.56 \pm 1.11	44.05 \pm 1.28	44.90	
4	2.82 \pm 0.12	2.48	0.21 \pm 0.06	0.41 \pm 0.10	0.62 \pm 0.12	0.31	0.46 \pm 0.06	0.49	2.36 \pm 0.11	4.43 \pm 0.23	6.79 \pm 0.26	7.08	
5	1.75 \pm 0.12	1.70	0.18 \pm 0.05	0.16 \pm 0.06	0.34 \pm 0.08	0.18	0.36 \pm 0.04	0.34	1.09 \pm 0.07	1.94 \pm 0.12	3.03 \pm 0.14	3.47	
6	2.24 \pm 0.11	1.93					0.43 \pm 0.04	0.38	1.13 \pm 0.07 ^c	1.86 \pm 0.10 ^c	2.99 \pm 0.12 ^c	2.99 ^c	
7	2.10 \pm 0.08	2.18					0.34 \pm 0.04	0.43	1.08 \pm 0.05 ^{b,c}	1.57 \pm 0.08 ^c	2.65 \pm 0.09 ^c	2.67 ^c	
8	1.54 \pm 0.07	1.33					0.29 \pm 0.04	0.26	0.54 \pm 0.03 ^c	0.76 \pm 0.04 ^c	1.30 \pm 0.05 ^c	1.03 ^c	
9	2.03 \pm 0.09	2.04					0.42 \pm 0.03	0.40	1.26 \pm 0.06 ^{c,d}	1.21 \pm 0.05 ^c	2.76 \pm 0.09 ^c	2.74 ^c	
10	1.44 \pm 0.07	1.44					0.17 \pm 0.03	0.28	0.29 \pm 0.04 ^c				
11	1.37 \pm 0.07	1.20					0.33 \pm 0.03	0.24	0.48 \pm 0.04 ^{c,e}	0.45 \pm 0.04 ^c	1.10 \pm 0.08 ^{c,g}	1.19 ^{c,g}	
12	1.38 \pm 0.07	1.25							0.07 \pm 0.03 ^c	0.40 \pm 0.04 ^c	0.47 \pm 0.05 ^c	0.67 ^c	
13	0.58 \pm 0.06	0.97					0.18 \pm 0.03	0.19	0.09 \pm 0.03 ^{c,f}				
14	0.64 \pm 0.06	0.74					0.16 \pm 0.03	0.15	0.03 \pm 0.03 ^{c,h}	0.25 \pm 0.04 ^c	0.36 \pm 0.07 ^{c,h}	0.32 ^{c,h}	
15	0.40 \pm 0.06	0.43					0.08 \pm 0.03	0.08	0.13 \pm 0.03 ^c	0.20 \pm 0.04 ^c	0.33 \pm 0.05 ^c	0.20 ^c	
16	0.21 \pm 0.06	0.28					0.07 \pm 0.03	0.06	0.15 \pm 0.03 ^c	0.11 \pm 0.04 ^c	0.26 \pm 0.05 ^c	0.11 ^c	
17	0.21 \pm 0.06	0.09					0.05 \pm 0.03	0.02	0.08 \pm 0.04 ^c				
18	0.26 \pm 0.06	0.26					0.09 \pm 0.03	0.05	0.05 \pm 0.03 ^c	0.16 \pm 0.04 ^c	0.21 \pm 0.05 ^c	0.10 ^c	
19	0.27 \pm 0.06	0.22							0.04 \pm 0.03 ^c				
20	0.27 \pm 0.06	0.21							0.04 \pm 0.03 ^c				
≥ 15	2.19 \pm 0.14												
≥ 21	0.57 \pm 0.12								0.16 \pm 0.04 ^c				
series limit	< 0.35 ⁱ												

^a Large error due to subtraction of ^{56}Mn γ line.

^b The $7d \rightarrow 2p_{1/2}$ intensity includes the $12p \rightarrow 2s$ intensity.

^c The $nd \rightarrow 2p_{1/2}$ intensities and the $nd \rightarrow 2p_{3/2}$ intensities include the $ns \rightarrow 2p_{1/2}$ and $ns \rightarrow 2p_{3/2}$ intensities, respectively, if $n \geq 6$.

^d The $9 \rightarrow 2p_{1/2}$ intensity includes the $10 \rightarrow 2p_{3/2}$ intensity.

^e The $11 \rightarrow 2p_{1/2}$ intensity includes the $13 \rightarrow 2p_{3/2}$ intensity.

^f The $13 \rightarrow 2p_{1/2}$ intensity includes the $17 \rightarrow 2p_{3/2}$ intensity.

^g The $11 \rightarrow 2p$ intensity includes the $13 \rightarrow 2p$ and $17 \rightarrow 2p$ intensities.

^h The $14 \rightarrow 2p_{1/2}$ and the $14 \rightarrow 2p$ intensities include the $19 \rightarrow 2p_{3/2}$ and $20 \rightarrow 2p_{3/2}$ intensities and the $19 \rightarrow 2p$ and $20 \rightarrow 2p$ intensities, respectively.

ⁱ Upper limit at 90% confidence for transitions from the continuum (0–1 keV energy) to the 1s level.

polated to $Z=26$ and also by solving the Dirac equation with an electron screening potential derived from Hartree-Fock calculations.⁹ Unresolved lines were decomposed into components at the calculated positions.

The largest uncertainty in screening is the occupation of the 2s electron states. Removal of one 2s electron changes¹⁰ muonic levels with $10 \leq n \leq 16$ by about 180 eV. We estimated conservatively the corresponding uncertainty to be < 150 eV yielding a relative intensity error of the respective muonic lines of < 5%. The hyperfine splitting due to the isotopic composition of Fe was taken into account. The total intensity of the Lyman series was set to 100%. Details will be given in a forthcoming paper.¹¹ Tables I and II summarize the results. An upper limit is given for transitions from the continuum (unbound muon) to the 1s level. Cascade calculations were

performed with a program⁶ taking, if wanted, the electron depletion into account.¹² The rate for refilling a vacancy in the electronic K shell is¹⁰ $1.6 \times 10^{15} \text{ sec}^{-1}$ (for $Z=25$) if all other electrons are present, and the corresponding L shell rate is $7 \times 10^{14} \text{ sec}^{-1}$. Since, with exception of the 2s life time, the average muonic cascade from $n_i=20$ is calculated to take about $1.5 \times 10^{-14} \text{ sec}$ total and not to empty the L shell completely, only K refilling was taken into account; the rate was limited to be $\leq 10^{16} \text{ sec}^{-1}$.

Normalized χ^2 values for various initial distributions and K refilling rates, with all parameters optimized, are given in Table III. Experimentally observed transitions with $n_u > 14$ are not taken into account in the calculations starting with $n_i = 14$. The distribution equation (1) does not reproduce the experimental data. A strong modification according to Eq. (2) improves the agreement

TABLE II. Experimental and calculated intensities of the muonic M , N , and O series in iron (per 100 stopped muons).

n	M series n → 3		N series n → 4		O series n → 5	
	exp.	calc.	exp.	calc.	exp.	calc.
4	33.21 ± 1.17	33.20				
5	7.80 ± 0.46	7.86	25.66 ± 1.75	24.63		
6	4.57 ± 0.37	4.47	5.63 ± 0.85	6.27	9.9 ± 5.0 ^a	13.78
7	2.55 ± 0.20	2.79	2.63 ± 0.14	2.81	2.62 ± 0.28	3.13
8	1.19 ± 0.10	1.00	1.54 ± 0.43	0.83	0.73 ± 0.06	0.74
9	1.93 ± 0.19	1.70	0.90 ± 0.22	1.39	1.14 ± 0.16	1.22
10	1.07 ± 0.17	0.89	0.82 ± 0.13	0.66	0.48 ± 0.06	0.53
11	0.68 ± 0.13	0.57	0.24 ± 0.10	0.41	0.45 ± 0.09	0.31
12	0.34 ± 0.06	0.57	0.26 ± 0.10	0.39	0.41 ± 0.06	0.29
13	0.23 ± 0.15	0.40	0.15 ± 0.03	0.27	0.24 ± 0.08	0.19
≥14	0.61 ± 0.10	0.75	0.32 ± 0.13	0.50		

^aLarge error due to subtraction of the Al 4 → 3 transition.

considerably. The best agreement was obtained for $n_i = 20$ with a quadratic approximation (last line of Table III); the intensities calculated with this input datum are listed in Tables I and II. This initial distribution does not strongly depend on l . It is not surprising that our K refilling rate is appreciably smaller than the literature value¹³ as the majority of the L electrons are emitted during the muonic cascade.

Full agreement between calculated and experimental intensities cannot be expected because the calculations are based on a two-parameter description of the initial distribution limited to one n_i value and many details such as electronic fine structure and outer-shell vacancies are not taken into account. Nevertheless the applied cascade program⁶ is shown to be a powerful tool. Even

the intensities of most transitions with $14 < n_u \leq 20$ are well reproduced. This indicates that only a minor portion of the muons can be directly captured in levels with $n_i < 20$. However, our results do not say at all that the muons are really captured with $n_i = 20$, since initial distribution as used here means only the distribution the cascade calculation starts with.

The rather flat initial distribution obtained from our experiment is not in agreement with predicted nearly statistical distributions.^{1,3,4} The gross features are reproduced however by the "fuzzy Fermi-Teller model"⁵ with an adapted parameter yielding a strongly enhanced collision rate of the muon with the electrons in the outer part of the atom.

We wish to thank Schweizerisches Institut für

TABLE III. Comparison with various cascade calculations.

Initial distribution type	$n_i = 14$			$n_i = 20$		
	Parameter	K refilling per sec	χ^2	Parameter	K refilling per sec	χ^2
$2l+1$ ^a	29 ^a	22
$2l+1$...	10^{16}	32	...	10^{16}	30
$(2l+1)e^{\alpha l}$	$\alpha = -0.12$... ^a	9.1	$\alpha = -0.08$... ^a	7.3
$(2l+1)e^{\alpha l}$	$\alpha = -0.135$	2×10^{14}	5.2	$\alpha = -0.11$	2×10^{14}	4.1
const ^a	19 ^a	9.4
const				...	4×10^{14}	5.2
$1+al$				$a = 0.02$	4×10^{14}	4.0
$1+al+bl^2$				$a = 0.14$ $b = -0.006$	2.5×10^{14}	3.6

^aNo reduction of the muonic Auger rate due to electronic depletion.

Nuklearforschung for hospitality and support, and H. Hagn for technical assistance. Financial support by the German Bundesministerium für Forschung und Technologie is acknowledged.

¹E. H. S. Burhop, in *High Energy Physics*, edited by E. H. S. Burhop (Academic, New York, 1969), Vol. 3, p. 109, and papers quoted there.

²H. Backe, *Z. Phys.* **241**, 435 (1971).

³P. Vogel, P. K. Haff, V. Akylas, and A. Winther, *Nucl. Phys.* **A254**, 445 (1975).

⁴M. Leon and R. Seki, Los Alamos Scientific Labora-

tory Report No. LA-UR-75-1267 (unpublished).

⁵M. Leon and J. H. Miller, Los Alamos Scientific Laboratory Report No. LA-UR-75-1268 (unpublished).

⁶Program CASCADE by J. Hüfner; *J. Hüfner, Z. Phys.* **195**, 365 (1966).

⁷A. Messiah, *Quantum Mechanics* (North-Holland, Amsterdam, 1964), Vol. 1, p. 241.

⁸P. Vogel, *At. Data Nucl. Data Tables* **14**, 599 (1974).

⁹Program HARTRY by P. Vogel.

¹⁰P. Vogel, *Phys. Rev. A* **7**, 63 (1973).

¹¹H. Daniel *et al.*, to be published.

¹²H. P. Povel, private communication.

¹³O. Keski-Rahkonen and M. O. Krause, *At. Data Nucl. Data Tables* **14**, 139 (1974).

Destructive Interference of Imaginary Resonant Contributions to $\chi^{(3)}$ †

Haim Lotem and R. T. Lynch, Jr.

Gordon McKay Laboratory, Harvard University, Cambridge, Massachusetts 02138

(Received 31 March 1976)

The first observation of destructive interference of imaginary contributions to $\chi^{(3)}$ from different resonances is reported. Destructive and constructive interferences were obtained between Raman and two-photon absorption (TPA) contributions in organic liquids. Accurate TPA and two-photon dispersion spectra of CS_2 obtained by using these interferences in $\chi^{(3)}$ are reported. The TPA experiment described is superior to the classical TPA experiments in its accuracy and in the fact that it lacks the uncertainties originating from scattering processes which compete with true TPA.

We report the first observation of destructive interference of imaginary contributions of different two-photon resonances to the complex nonlinear optical susceptibility $\chi^{(3)}$. It is shown that destructive and constructive interference can be achieved simply by interchanging the frequencies of the laser beams used in the measurements of $\chi^{(3)}$. Important uses are discussed for the reported interference effects in determinations of accurate absolute values for two-photon absorption (TPA) cross sections. We emphasize that

the interferences reported here are between different two-photon contributions to $\chi^{(3)}$, possibly even from different materials. Bjorkholm and Liao^{1a} and Stein *et al.*^{1b} have observed destructive interference among the contributions of one-photon levels to a *single* TPA or Raman term, respectively.

The two experiments used for demonstrating the interference between the imaginary terms are specific examples of parametric mixing, where three electromagnetic fields $\vec{E}(i)$ ($i = a, b, c$) produce a nonlinear polarization given by²

$$P_j^{(3)}(\omega_{\text{out}} = \omega_a + \omega_b + \omega_c) = \chi_{ijklm}^{(3)}(-\omega_{\text{out}}, \omega_a, \omega_b, \omega_c) E_k(\omega_a) E_l(\omega_b) E_m(\omega_c). \quad (1)$$

This polarization generates a new field at ω_{out} .

In general, the third-order susceptibility $\chi^{(3)}(-\omega_{\text{out}}, \omega_a, \omega_b, \omega_c)$ controls "four-photon" or "four-wave" processes. We consider here two specific cases, $\omega_{\text{out}} = \omega_1 + \omega_1 - \omega_2$ and $\omega_{\text{out}} = \omega_1 - \omega_1 + \omega_2$. The former involves three different waves and has been called three-wave mixing (3WM).³ The latter we shall call the "Kerr effect" (KE) susceptibility. The name Kerr effect is most appropriate for the off-diagonal elements of $\chi^{(3)}(-\omega_2, \omega_1, -\omega_1, \omega_2)$ since these control the effective rotation of the polarization of the beam at ω_2 due to the presence of light at ω_1 . Even though the third-order nonlinear susceptibilities are measured in parametric experiments where the material system does not change its quantum state, the importance of these susceptibilities is that different resonant contributions to $\chi^{(3)}$ are proportional to corresponding nonparametric two-photon scattering cross sections.² That is, when an in-